Statistical Modeling and Classification of Reflectance Confocal Microscopy Images

Abdelghafour Halimi[(1)] , Hadj Batatia[(1)], Jimmy Le Digabel[(2)], Gwendal Josse[(2)] and Jean-Yves Tourneret[(1)]
[1]University of Toulouse, ENSEEIHT-IRIT, 2 rue Camichel, BP 7122, 31071 Toulouse cedex 7, France
[2]Centre de Recherche sur la Peau, Pierre Fabre Dermo-Cosmétique, 2 rue Viguerie, 31025 Toulouse Cedex 3

***Abstract*—This paper deals with the characterization and classification of reflectance confocal microscopy images of human skin. A special attention will be given to the identification and characterization of the lentigo, a phenomenon that originates at the dermo-epidermic junction of the skin. Confocal images are acquired at different skin depths with a high resolution. For each depth, the histograms of pixel intensities are determined, and well statistically modelled with a generalized gamma distribution (GGD). The scale, shape and translation parameters associated with the GGD are estimated using a new natural gradient descent algorithm showing fast convergence properties when compared to state-of-the-art estimation methods. Results show that the estimated parameters can be used to classify clinical images of lentigo and healthy patients. They also show that the scale and shape parameters are good features to identify and characterize the presence of lentigo in skin tissues.**

Keywords*—*Reflectance confocal microscopy, lentigo characterization, maximum likelihood estimation, natural gradient.

I. Introduction

The human skin is a large and complex organ that can be subjected to a number of diseases. The lentigo is a lesion that originates at the junction between the dermis and the epidermis due to a high concentration of melanocytes aggregating at the dermal papillae walls. This lesion leads to the destruction of the regular cellular network at the dermoepidermal junction [1]. The diagnosis of lentigo can be performed through visual inspection or through biopsy of the skin surface. Reflectance confocal microscopy (RCM) is a non-invasive imaging technique that enables in vivo visualisation of the epidermis down to the papillary dermis in real time [2], [3]. Its potential to improve the detection of cancer and tumors has been demonstrated in various research and dermatological clinical studies [4]. Current practices to analyze these images are mainly based on visual inspection. However, the automatic analysis of confocal images is also very interesting. In [5], a correlation between RCM and histology has been reported for the diagnosis of melanoma. RCM has also been proved valuable for treatment follow up [6], guidance of cutaneous surgery [7], and surveillance of lentigo maligna treatment [8], [9].

The complex nature of RCM images requires automatic image processing methods to build accurate diagnosis strategies. Recent research on RCM images has mainly focused on three aspects: i) clinical studies to evaluate their usefulness, ii) segmentation of nuclei, and iii) classification of skin tissues. Luck et al. [10] have first developed an automatic RCM image processing method to segment nuclei. Their method was based on a Gaussian image model that takes into account the reflectivity of nuclei and a truncated Gaussian distribution to represent the intensity of the cytoplasm fibers. A Gaussian Markov random field was also used for spatial correlation, and a Bayesian classification algorithm was investigated to label tissues. Neural networks were also used to perform nuclei segmentation in RCM images as described in [11]. Various features extracted from RCM images have been used for the applications cited above. Kurugol et al. [12], [13] developed and validated a semi-automatic method to locate the dermoepidermal junction (DEJ) using a statistical classifier based on texture features. Texture analysis was also considered in [14] to localize skin layers in RCM images. Hames et al. [15], [16] developed a logistic regression classifier to automatically segment the different layers of the skin in RCM images. In [17], a support vector machine (SVM) classifier based on SURF texture features was proposed to identify skin morphological patterns in RCM images. Finally, Koller et al. [18] investigated a wavelet-based decision tree classification method to distinguish benign and malignant melanocytic skin tumors in RCM images. This method, will be used as a benchmark in our study.

The first contribution of this paper is a statistical model that allows the characterization of the underlying tissues. The variability of the pixel intensities of an RCM image is represented by a GGD, whose parameters are used as features for the classification of healthy and lentigo confocal images. The representation of the confocal images into a 3D space of parameters acts as an interesting dimension reduction technique allowing classification algorithms to be implemented in quasi real-time. The GGD statistical model is adjusted to the intensities of the RCM images at different depths, to identify the skin depths at which lentigo detection and characterization are the most significant. A quantitative analysis supported by an SVM classifier is conducted to evaluate the performance of the proposed characterization. A second contribution of this work is a new estimation algorithm for the GGD parameters, based on a natural gradient approach [19]. The main property of this algorithm is its fast convergence compared to other existing techniques, allowing big databases to be processed with reduced computational cost. This approach is also known as Fisher scoring [20]. It updates the parameters in a Riemannian space, resulting in a fast convergence to a local minimum of the cost function of interest [21]. The proposed model and estimation algorithm are validated using synthetic and real RCM images, resulting from a clinical study containing healthy and lentigo patients. The obtained results are very promising.

The paper is organized as follows. Section 2 presents the proposed method for lentigo detection and characterization and the proposed estimation algorithm based on a natural gradient method. Simulation results are presented and analyzed in Section 3. Conclusions and perspectives for future works are finally reported in Section 4.

II. Lentigo detection and characterization

This section presents the proposed approach based on the use of a GGD model for the image pixels to characterize and classify healthy and lentigo RCM images. It contains two steps that are summarized in Fig. 1 and described in the next sections.

978-1-5386-1251-4/17/$31.00 ©2017 IEEE

Fig. 1. Proposed classification method for lentigo and healthy confocal images.

A. Statistical estimation

1) Generalized gamma distribution: In this paper, we propose to use the statistical properties of the pixel intensities to detect the presence of lentigo in RCM images. More precisely, we consider a vectorized RCM image denoted as $\boldsymbol{x} = (x_1, \ldots, x_N)$ associated with N pixels and we assume that the distribution of these pixel intensities is a GGD [22], [23]. The GGD depends on the parameter vector $\boldsymbol{\theta} = (\gamma, \beta, \rho)^T$ and is defined as

$$f(x_n; \boldsymbol{\theta}) = \frac{(x_n - \gamma)^{\rho-1}}{\beta^{\rho}\,\Gamma(\rho)} \exp\left(-\frac{x_n - \gamma}{\beta}\right) \mathcal{I}_{]\gamma,+\infty[}(x_n) \quad (1)$$

where $\mathcal{I}_A$ is the indicator function on the set A, $\beta > 0, \rho > 0$ and $\Gamma(.)$ is the gamma function [24]. We will show in Section III-A2 that the density (1) is perfectly adapted to the distribution of RCM images. The next section introduces a new statistical estimation method based on the maximum likelihood (ML) principle and the natural gradient descent. This method allows the parameter vector $\boldsymbol{\theta}$ to be estimated from the samples x_n.

2) ML estimation: The ML estimation method consists of maximizing the likelihood of the observed samples with respect to the unknown model parameters [25]. Assuming that the observations x_n are independent, the likelihood function of the sample $\boldsymbol{x} = (x_1, ..., x_N)^T$ is defined as

$$f(\boldsymbol{x}; \boldsymbol{\theta}) = \prod_{n=1}^{N} f(x_n; \boldsymbol{\theta}) \quad (2)$$

leading to the following log-likelihood function

$$\mathcal{L}(\boldsymbol{\theta}) = \log\left[f(\boldsymbol{x}; \boldsymbol{\theta})\right] = -N\rho\, \log(\beta) - N\, \log\left[\Gamma(\rho)\right] + (\rho - 1)\sum_{n=1}^{N} \log(x_n - \gamma) - \frac{1}{\beta}\sum_{n=1}^{N}(x_n - \gamma). \quad (3)$$

The partial derivatives of the log-likelihood with respect to γ, β and ρ can be computed easily leading to

$$\begin{cases} \frac{\partial\, \mathcal{L}(\boldsymbol{\theta})}{\partial \gamma} = -(\rho - 1)\, \sum_{n=1}^{N}(x_n - \gamma)^{-1} + \frac{N}{\beta} \\ \frac{\partial\, \mathcal{L}(\boldsymbol{\theta})}{\partial \beta} = \frac{-N\rho}{\beta} + \frac{1}{\beta^2}\sum_{n=1}^{N}(x_n - \gamma) \\ \frac{\partial\, \mathcal{L}(\boldsymbol{\theta})}{\partial \rho} = -N\Psi(\rho) - N\, \log(\beta) + \sum_{n=1}^{N} \log(x_n - \gamma) \end{cases} \quad (4)$$

where $\Psi(z) = \Gamma'(z)/\Gamma(z)$ is the digamma function [24]. The maximization of the log-likelihood in (3) with respect to $\boldsymbol{\theta}$ can be conducted using various numerical algorithms. Jonkman and al. [23] proposed to use a gradient descent algorithm defined by the following recursion

$$\boldsymbol{\theta^{t+1}} = \boldsymbol{\theta^t} + \lambda A(\boldsymbol{\theta^t}) \nabla\, \mathcal{L}(\boldsymbol{\theta^t}) \quad (5)$$

where ∇ is the gradient operator, λ is an appropriate stepsize and A a preconditioning matrix that depends on $\boldsymbol{\theta^t}$ (e.g., defined from the Hessian of the log-likelihood).

In this paper, we consider another route defined by a natural gradient descent method in order to estimate the parameter vector $\boldsymbol{\theta}$. Contrary to Newton's method, a natural gradient recursion does not assume a locally-quadratic cost function and has the nice property to be asymptotically Fisher-efficient for ML estimation [19]. The main idea is to update the parameters in a Riemannian space, resulting in a fast convergence to a local minimum of the objective function [21]. The natural gradient recursion is defined by

$$\boldsymbol{\theta^{t+1}} = \boldsymbol{\theta^t} + \frac{\lambda}{\parallel F^{-1}(\boldsymbol{\theta^t}) \nabla \mathcal{L}(\boldsymbol{\theta^t}) \parallel} F^{-1}(\boldsymbol{\theta^t})\, \nabla\, \mathcal{L}(\boldsymbol{\theta^t}) \quad (6)$$

where $\nabla \mathcal{L}(\boldsymbol{\theta^t})$ is the gradient defined in (4) and $F(\boldsymbol{\theta^t})$ is the Fisher information matrix (FIM) defined as

$$F(\boldsymbol{\theta^t}) = -\begin{pmatrix} E\left(\frac{\partial^2 \mathcal{L}(\boldsymbol{\theta^t})}{\partial \gamma^2}\right) & E\left(\frac{\partial^2 \mathcal{L}(\boldsymbol{\theta^t})}{\partial \gamma\ \partial \beta}\right) & E\left(\frac{\partial^2 \mathcal{L}(\boldsymbol{\theta^t})}{\partial \gamma\ \partial \rho}\right) \\ E\left(\frac{\partial^2 \mathcal{L}(\boldsymbol{\theta^t})}{\partial \beta\ \partial \gamma}\right) & E\left(\frac{\partial^2 \mathcal{L}(\boldsymbol{\theta^t})}{\partial \beta^2}\right) & E\left(\frac{\partial^2 \mathcal{L}(\boldsymbol{\theta^t})}{\partial \beta\ \partial \rho}\right) \\ E\left(\frac{\partial^2 \mathcal{L}(\boldsymbol{\theta^t})}{\partial \rho\ \partial \gamma}\right) & E\left(\frac{\partial^2 \mathcal{L}(\boldsymbol{\theta^t})}{\partial \rho\ \partial \beta}\right) & E\left(\frac{\partial^2 \mathcal{L}(\boldsymbol{\theta^t})}{\partial \rho^2}\right) \end{pmatrix}. \quad (7)$$

Straightforward computation lead to

$$F(\boldsymbol{\theta}) = N \begin{pmatrix} \frac{1}{\beta^2(\rho-2)} & \frac{1}{\beta^2} & \frac{1}{\beta(\rho-1)} \\ \frac{1}{\beta^2} & \frac{\rho}{\beta^2} & \frac{1}{\beta} \\ \frac{1}{\beta(\rho-1)} & \frac{1}{\beta} & \Psi'(\rho) \end{pmatrix} \quad (8)$$

where Ψ' denotes the trigamma function [24]. The interest of using this natural gradient method for generalized gamma distributions will be clarified in Section III-A. To our knowledge, it is the first time that a natural gradient method is applied to generalized gamma distributions.

B. Characterization and classification

In order to characterize the presence of lentigo in RCM images, we can fit the GGD to RCM images at different depths. The resulting estimated parameters γ, β and ρ can be used to identify the skin depths at which lentigo detection and characterization are the most significant. The estimated GGD parameters associated with these characteristic depths can then be used to classify the healthy from lentigo patients using an SVM classification algorithm [26]. Simulation results confirming these properties are presented in Section III-B.

III. Simulation Results

A. Performance of the proposed estimation algorithm

1) Synthetic data: This section evaluates the performance of the proposed estimation algorithm on synthetic data. All simulations were conducted using MATLAB R2014b on a PC with an Intel(R) Core(TM) i7-4860HQ CPU 2.4 GHz processor, 32 GB RAM, and an Nvidia GeForce GTX 980m graphics card. In the first experiment, we generated samples distributed according to a GGD with a number of samples varying from $N = 40$ to $N = 1000$ using (1) with the following fixed parameters $\boldsymbol{\theta} = (\gamma, \beta, \rho)^T = (2, 15, 4)^T$ (note that additional results of other experiments are available in the technical report [27]) and $M = 1000$ Monte Carlo runs. The method investigated in [23] based on a Newton gradient descent using the Hessian as a pre-conditioned matrix was considered as a benchmark. A second method (referred to as analytical method) consists of using the two first equations of (4) to express β and ρ as a function of γ, i.e.,

$$\beta = \frac{\left[\sum_{n=1}^{N}(x_n - \gamma)\, \sum_{n=1}^{N}\left(\frac{1}{x_n^l - \gamma}\right)\right] - N^2}{N\, \sum_{n=1}^{N}\left(\frac{1}{x_n - \gamma}\right)}$$

$$\rho = \frac{\sum_{n=1}^{N}(x_n-\gamma)\ \sum_{n=1}^{N}\left(\frac{1}{x_n-\gamma}\right)}{\left[\sum_{n=1}^{N}(x_n-\gamma)\ \sum_{n=1}^{N}\left(\frac{1}{x_n-\gamma}\right)\right]-N^2}.$$

After replacing these expressions in the third equation of (4), we obtain a non-linear equation of γ defined as

$$-N\Psi(\rho) - N\ \log(\beta) + \sum_{n=1}^{N}\log(x_n-\gamma) = 0 \qquad (9)$$

which can be solved using a Newton gradient descent.

The RMSEs of the parameter estimates are displayed in log scale (to improve readability) in Fig. 2 with the associated running times. Note that the three methods were initialized with the same estimator based on the "pseudo method of moments" (see [23] for details). The proposed descent algorithm based on a natural gradient recursion provides smaller RMSEs for a small number of samples, i.e, for $N \in \{40, ..., 300\}$. The natural gradient descent also provides a faster convergence compared to the other methods with a significant reduction in computational cost for any sample size. This result is interesting since it allows big databases of RCM images to be processed more easily. These results highlight the good performance of the proposed strategy for the estimation of GGD parameters.

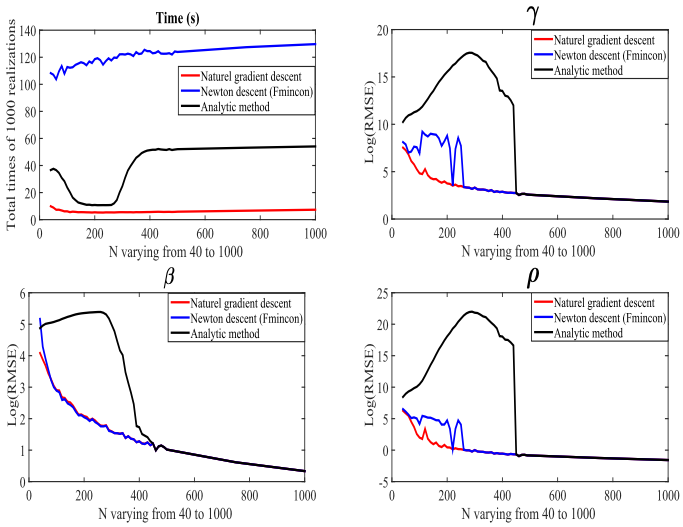

Fig. 2. RMSEs and total computational times for the three estimation methods for N varying from 40 to 1000.

2) Real data: This section is devoted to the validation of the proposed algorithm using real RCM images. The images were acquired with an apparatus Vivascope 1500, from the stratum corneum, the epidermis layer, the dermis-epidermis junction (DEJ) and the upper papillary dermis. Each RCM image shows a $500\times500\mu m$ field of view with 1000×1000 pixels. A set of $L = 45$ women aged 60 years and over were recruited. All the volunteers gave their informed consent for examination of skin by RCM. The volunteers were then divided into two groups according to the clinical evaluation performed by a physician. The first group was formed by 27 women with at least 3 lentigines on the back of the hand while 18 women without lentigo constituted the control group. Two acquisitions were performed on each volunteer for the 25 depths, each acquisition providing a so-called stack containing the 25 images. Images were taken on lentigo lesions for volunteers of the first group and on healthy skin on the back of the hand for the control

TABLE I. ESTIMATED GGD PARAMETERS ASSOCIATED WITH THE GGDS DISPLAYED IN FIG. 3.

	Healthy			Lentigo		
Depth	$\widehat{\gamma}$	$\widehat{\beta}$	$\widehat{\rho}$	$\widehat{\gamma}$	$\widehat{\beta}$	$\widehat{\rho}$
Z = 45μm	4.59	4.96	4.51	4.27	7.19	3.81
Z = 54μm	4.63	4.79	4.09	2.70	7.03	3.74
Z = 67.5μm	3.68	4.73	4.30	2.51	7.59	3.11

group. An examination of each acquisition has been performed in order to locate the stratum corneum and the DEJ precisely in each image. Consequently, our database contained $L = 45$ patients. For each patient, we considered two stacks of 25 RCM images, giving a total of 2250 images. Fig. 3 compares the histograms of the RCM image intensities with the estimated GGD distributions at 3 representative depths. This figure corresponds to two arbitrary healthy and lentigo patients. The GGD is clearly a good statistical model for the RCM image intensities, for both lentigo and healthy images. Table I shows that the estimated scale and shape parameters of the distributions associated with healthy and lentigo images are significantly different, allowing these images to be classified. In addition to showing that the GGD captures well the statistical properties of RCM images, our method allows identifying the depth at which the lentigo is best discriminated, which will be the focus of the next section.

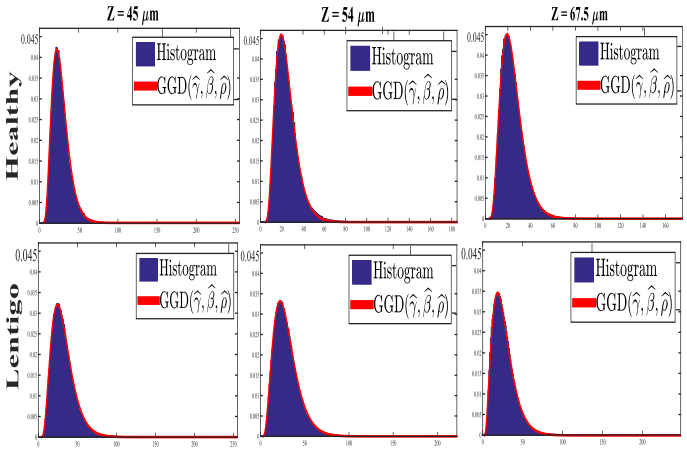

Fig. 3. Histograms of the RCM image intensities. The figure corresponds to data from two arbitrary healthy and lentigo patients (patients #6 and #38) at three representative depths (one depth per column).

B. Identification of characteristic depths

The GGD distributions were fitted to each of the 2250 images. Having acquired two stacks of 25 images for each patient, one of the two stacks was selected randomly for the analysis. The averaged estimated parameters $\overline{\boldsymbol{\theta}}_{\text{Healthy}}$ and $\overline{\boldsymbol{\theta}}_{\text{Lentigo}}$ were then calculated at each depth for healthy and lentigo patients. To account for variability, the process of selecting one stack for each patient was repeated 300 times. The averaged results and the corresponding standard deviations are displayed in Fig. 4, which clearly shows that β and ρ allow the discrimination of healthy and lentigo patients for depths between $40\mu m$ and $60\mu m$, with a maximal difference around $50\mu m$. Conversely, parameter γ does not allow healthy and lentigo patients to be distinguished. As mentioned in the introduction, lentigines are mainly characterized in RCM images by the disorganization of the

dermoepidermal junction (DEJ). This explains why parameter β is very discriminant at depths close to $50\mu m$, which corresponds to the average depth that represent the DEJ (the true DEJ interval was annotated by the dermatologists and is delimited by the two blue lines) as shown in Fig. 5. This result is compatible with clinical practices for analyzing the DEJ, confirming the validity of our approach.

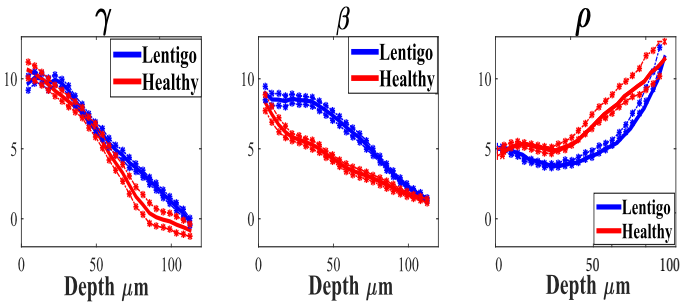

Fig. 4. Evolution of the averaged estimated parameters $\hat{\gamma}$, $\hat{\beta}$ and $\hat{\rho}$ versus depth.

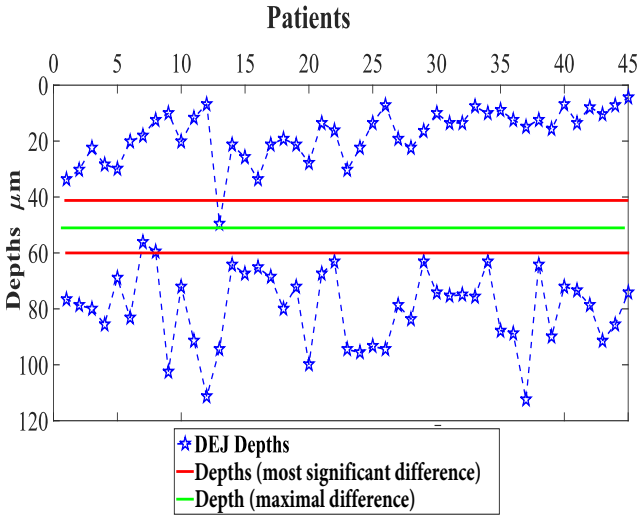

Fig. 5. Estimated characteristic depths located between 40μm and 60μm (green and red lines) and the true DEJ depths annotated by the dermatologists (blue lines) associated with the 45 patients.

C. Classification performance

Section III-B provided an estimate of the depths allowing healthy and lentigo patients to be classified. An SVM classification algorithm was considered in this section in order to confirm these results. The estimated GGD parameters associated with the characteristic depths $(40\mu m$ to $60\mu m)$ for a given patient were then used to classify the patients into 2 classes referred to as "lentigo" and "healthy". The leave-one-out method was used to compute the different error probabilities. This method uses $L-1$ images for training (where L is the number of patients in the database) and the remaining image for testing. This operation is repeated $M = 1000$ times to determine the probabilities of error and of correct classification. For each experiment, we considered only images from one acquisition out of the two (for each patient). The M results were then used to calculate the average confusion matrix shown in Table II and to evaluate the average indicators (Precision, Specificity, Sensitivity and Accuracy). These indicators are defined as Precision = TP/(TP+FP), Specificity = TN/(FP+TN), Sensitivity = TP/(TP+FN), Accuracy = (TP+TN)/(TP+FN+FP+TN), where TP, FP, TN and FN are the numbers of true positives, false positives, true negatives, and false negatives. This table allows us to evaluate the classification performance for these characteristic depths. The accuracy for the classification of healthy and lesion tissues is equal to 84.4 % for β and to 82.2 % for ρ (the results concerning the parameter ρ are not shown here for brevity and can be found in [27]), confirming that these parameters can be used for lentigo detection. Fig. 6 shows examples of RCM images classified using the proposed methodology. The method presented in [18] was then compared to our algorithm in order to assess the significance of our results. This method consists of extracting from each RCM image a set of 39 parameters (more technical details are available in [28]) and applying to these features a classification procedure based on a classification and regression tree (CART). Note that the CART algorithm was tested on the real RCM images using a leave one out procedure. As shown in Table II, the accuracy obtained with the CART algorithm is 80%, i.e., it is slightly smaller than the one obtained with the proposed method and leads to two additional mis-classified patients. Furthermore, the estimated GGD parameters can be used for the characterization of RCM images, which is not possible with CART.

TABLE II. CLASSIFICATION PERFORMANCE ON REAL RCM IMAGES (45 PATIENTS).

	β			CART method		
Confusion matrix	$\hat{L}$	$\hat{H}$	Sensitivity Specificity	$\hat{L}$	$\hat{H}$	Sensitivity Specificity
Lentigo	22	5	81.4 %	21	6	77.7 %
Healthy	2	16	88.8 %	3	15	83.3 %
Precision	91.6 %	76.1 %		87.5 %	71.4 %	
Accuracy	84.4 %			80 %		

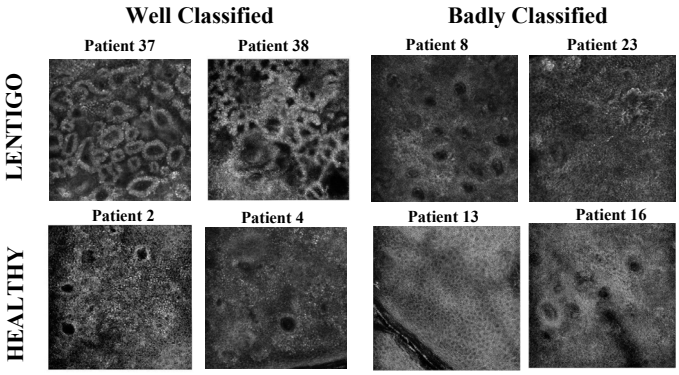

Fig. 6. Examples of RCM images (at the depth 58.5 μm) for lentigo and healthy patients classified by the proposed SVM method.

IV. CONCLUSIONS

This paper investigated the potential of using the statistical properties of reflectance confocal microscopy images to classify healthy and lentigo skins. The proposed method estimated the parameters of a generalized gamma distribution for the RCM images. These parameters were then used to train an SVM classifier. The proposed classifier was tested on a database of 2250 real images associated with 45 patients yielding promising results. Future work will be devoted to the segmentation of these RCM images using the estimated parameters of the GGD distributions.

REFERENCES

[1] S. González, *Reflectance confocal microscopy of cutaneous tumors*. CRC Press, 2017.

[2] P. Calzavara-Pinton, C. Longo, M. Venturini, R. Sala, and G. Pellacani, "Reflectance confocal microscopy for in vivo skin imaging," *Photochemistry and photobiology*, vol. 84, no. 6, pp. 1421–1430, 2008.

[3] R. Hofmann-Wellenhof, E. Wurm, V. Ahlgrimm-Siess, E. Richtig, S. Koller, J. Smolle, and A. Gerger, "Reflectance confocal microscopy-state-of-art and research overview," *Seminars in Cutaneous Medecine and Surgery, Elsevier*, vol. 28, pp. 172–179, 2009.

[4] I. Alarcon, C. Carrera, J. Palou, L. Alos, J. Malvehy, and S. Puig, "Impact of in vivo reflectance confocal microscopy on the number needed to treat melanoma in doubtful lesions," *British journal of Dermatology.*, vol. 170, pp. 802–808, 2014.

[5] T. D. Menge, B. P. Hibler, M. A. Cordova, K. S. Nehal, and A. M. Rossi, "Concordance of handheld reflectance confocal microscopy (rcm) with histopathology in the diagnosis of lentigo maligna (lm): A prospective study," *J. Am. Acad. Dermatol.*, vol. 74, no. 6, pp. 1114–1120, 2016.

[6] I. Alarcon, C. Carrera, L. Alos, J. Palou, J. Malvehy, and S. Puig, "In vivo reflectance confocal microscopy to monitor the response of lentigo maligna to imiquimod," *J. Am. Acad. Dermatol.*, vol. 71, pp. 49–55, 2014.

[7] B. P. Hibler, M. Cordova, R. J. Wong, and A. M. Rossi, "Intraoperative real-time reflectance confocal microscopy for guiding surgical margins of lentigo maligna melanoma," *Dermatologic Surgery.*, vol. 41, pp. 980–983, 2015.

[8] P. Guitera, L. Haydu, S. Menzies, and al, "Surveillance for treatment failure of lentigo maligna with dermoscopy and in vivo confocal microscopy: new descriptors." *British journal of Dermatology.*, vol. 170, pp. 1305–1312, 2014.

[9] J. Champin, J. Perrot, E. Cinotti, B. Labeille, C. Douchet, G. Parrau, F. Cambazard, P. Seguin, and T. Alix, "In vivo reflectance confocal microscopy to optimize the spaghetti technique for defining surgical margins of lentigo maligna," *Dermatologic Surgery*, vol. 40, no. 3, pp. 247–256, 2014.

[10] B. Luck, K. Carlson, A. Bovik, and R. Richards-Kortum, "An image model and segmentation algorithm for reflectance confocal images of in vivo cervical tissue," *IEEE Trans. Image Processing*, vol. 14, no. 9, pp. 1265–1276, 2005.

[11] M. Harris, A. Van, B. Malik, J. Jabbour, and K. Maitland, "A pulse coupled neural network segmentation algorithm for reflectance confocal images of epithelial tissue," *PloS one*, vol. 10, no. 3, p. e0122368, 2015.

[12] S. Kurugol, M. Dy, J.G.and Rajadhyaksha, K. Gossage, J. Weissmann, and D. Brooks, "Semi-automated algorithm for localization of dermal/epidermal junction in reflectance confocal microscopy images of human skin," in *SPIE BiOS*. International Society for Optics and Photonics, 2011, pp. 79 041A–79 041A–10.

[13] S. Kurugol, M. Rajadhyaksha, J. Dy, and D. Brooks, "Validation study of automated dermal/epidermal junction localization algorithm in reflectance confocal microscopy images of skin," in *SPIE BiOS*. International Society for Optics and Photonics, 2012, pp. 820 702–820 702–11.

[14] E. Somoza, G. Cula, C. Correa, and J. Hirsch, *Automatic Localization of Skin Layers in Reflectance Confocal Microscopy*. Cham: Springer International Publishing, 2014, pp. 141–150. [Online]. Available: http://dx.doi.org/10.1007/978-3-319-11755-3_16

[15] S. C. Hames, M. Ardigo, H. P. Soyer, A. P. Bradley, and T. W. Prow, "Anatomical skin segmentation in reflectance confocal microscopy with weak labels," in *Proc. Int. Conf. Dig. Image Comput. (dICTA'2015)*, Adelaide, AUS, 2015, pp. 1–8.

[16] S. C. Hames, M. Ardigò, H. P. Soyer, A. P. Bradley, and T. W. Prow, "Automated segmentation of skin strata in reflectance confocal microscopy depth stacks," *PloS one*, vol. 11, no. 4, p. e0153208, 2016.

[17] K. Kose, C. Alessi-Fox, M. Gill, J. Dy, D. Brooks, and M. Rajadhyaksha, "A machine learning method for identifying morphological patterns in reflectance confocal microscopy mosaics of melanocytic skin lesions in-vivo," in *SPIE BiOS*. International Society for Optics and Photonics, 2016, pp. 968 908–968 908–8.

[18] S. Koller, M. Wiltgen, V. Ahlgrimm-Siess, W. Weger, R. Hofmann-Wellenhof, E. Richtig, J. Smolle, and A. Gerger, "In vivo reflectance confocal microscopy: automated diagnostic image analysis of melanocytic skin tumours," *Journal of the European Academy of Dermatology and Venereology*, vol. 25, no. 5, pp. 554–558, 2011.

[19] S. Amari and S. Douglas, "Why natural gradient?" in *IEEE Int. Conf. Acoust., Speech, and Signal Processing (ICASSP)*, vol. 2, Seattle, WA, May 1998, pp. 1213–1216.

[20] A. Halimi, C. Mailhes, J.-Y. Tourneret, and H. Snoussi, "Bayesian estimation of smooth altimetric parameters: Application to conventional and delay/doppler altimetry," *IEEE Transactions on Geoscience and Remote Sensing*, vol. 54, no. 4, pp. 2207–2219, 2016.

[21] M. Pereyra, H. Batatia, and S. McLaughlin, "Exploiting information geometry to improve the convergence properties of variational active contours," *IEEE Journal of Selected Topics in Signal Processing*, vol. 7, no. 4, pp. 700–707, 2013.

[22] N. Johnson, S. Kotz, and N. Balakrishnan, *Continuous Univariate Distributions, vol. 1*. Wiley Series in Probability and Statistics, 1994.

[23] J. Jonkman, P. Gerard, and W. Swallow, "Estimating probabilities under the three-parameter gamma distribution using composite sampling," *Computational Statistics & Data Analysis*, vol. 53, no. 4, pp. 1099–1109, February 2009.

[24] M. Abramowitz and I. Stegun, *Handbook of Mathematical functions with Formulas, Graphs and Mathematical Tables*. Dover Publications, 1970.

[25] S. Kay, *Fundamentals of Statistical Signal Processing: Estimation Theory*. Englewood Cliffs, NJ: Prentice-Hall, 1993.

[26] S. R. Gunn *et al.*, "Support vector machines for classification and regression," *ISIS technical report*, vol. 14, pp. 85–86, 1998.

[27] A. Halimi, H. Batatia, J. L.Digabel, G. Josse, and J.-Y. Tourneret, "Technical report associated with the paper "Statistical modeling and classification of reflectance confocal microscopy images"," University of Toulouse, France, Tech. Rep., April 2017. [Online]. Available: https://arxiv.org/submit/1916290

[28] M. Wiltgen, A. Gerger, C. Wagner, J. Smolle *et al.*, "Automatic identification of diagnostic significant regions in confocal laser scanning microscopy of melanocytic skin tumors," *Methods of Information in Medicine*, vol. 47, no. 1, pp. 14–25, 2008.